Pergamon

Acta mater. Vol. 46, No. 1, pp. 91–99, 1998

Printed in Great Britain
PII: S1359-6454(97)00228-0
1359-6454/98 $19.00 + 0.00

KINETIC UNDERCOOLING IN SOLIDIFICATION OF A HYPEREUTECTIC Al–Si ALLOY; EFFECT OF SOLIDIFYING WITHIN A CERAMIC PREFORM COMPOSITE

A. SUNDARRAJAN[1], A. MORTENSEN*[1], T. Z. KATTAMIS[2] and M. C. FLEMINGS[1]

[1]Department of Materials Science and Engineering, Massachusetts Institute of Technology, Cambridge, MA 02139 and [2]Department of Metallurgy, University of Connecticut, Storrs, CT 06268, U.S.A.

(Received 30 December 1996; accepted 18 July 1997)

Abstract—Dendrite tip temperature measurements are reported for the hypereutectic alloy Al–30% Si, directionally solidified as a bulk (non-composite) alloy, and also as the matrix of a fibrous metal matrix composite. Over the range of tip velocities studied (10–1000 μm s) the primary Si tip undercooling in the directionally solidified bulk alloy increases slightly with increasing tip velocity, and indicates, by its large value, the presence of significant kinetic undercooling. This is in contrast with solidification of the composite, in which the primary Si tip undercooling decreases markedly with increasing tip velocity and is in quantitative agreement with theory for cellular solidification with no kinetic undercooling. These results, supported by metallographic observations, indicate that "wetting" of the alumina fibers by the growing silicon phase in the composite essentially eliminates the kinetic barrier to growth of primary Si crystals. The underlying mechanism is rationalized on the basis of macroscopic capillaric analysis at the solid/fiber/liquid juncture. This juncture is shown to be significantly more efficient in nucleating new facet planes than is a re-entrant twin plane corner. © *1997 Acta Metallurgica Inc.*

1. INTRODUCTION

The reinforcement of a metal with a high volume fraction of a chemically inert solid phase can change its solidification behavior significantly. Geometrical restrictions and capillary phenomena caused by the reinforcement can result in alterations of matrix coarsening, microsegregation, tip undercooling, and final solidification microstructure. As a result, the microstructure of the metal matrix in a composite produced by solidification processing can be very different from that found in the analogous unreinforced metal solidified under identical conditions. This has motivated interest in the solidification of metal matrix composites, most research to date having been conducted using aluminum-based alloys or transport metal analogues to elucidate and analyze several of its main governing phenomena. Research on the solidification of metal matrix composites is reviewed in Refs [1–4].

Capillary forces exert a particularly strong influence in this class of solidification problems: in addition to capillary phenomena associated with the presence of the interface separating the growing solid from the liquid, there are, in composites, capillary forces created by the presence of the reinforcement. Of particular importance in this regard is the contact angle θ of the primary solid metal on the reinforcement in the presence of the liquid metal. This angle θ is the same as that which is considered in the elementary treatment of the thermodynamics of heterogeneous nucleation, and characterizes the energetic attraction between the reinforcement and the growing primary solid within the liquid.

In most cast metal matrix composites of practical interest the matrix is aluminum-rich, and θ has been found to be large, near 180°. Nucleation of the solid phase is then not catalyzed by the reinforcement, and primary solid grows away from the reinforcement. This latter effect was shown using directional solidification experiments for Al–Cu alloys reinforced with aluminum oxide fibers [5] or SiC fibers [6]. In some cases, however, there is evidence that θ is small. The growing solid phase then tends to nucleate on the reinforcement, and is expected to grow along the matrix/reinforcement interface [4]. The most practically important among such metal matrix composite systems is that of reinforced hypereutectic Al–Si alloys: primary Si nucleates preferentially on graphite, SiC, SiO_2, and Al_2O_3 reinforcements [2, 7], indicating that θ is low between this primary phase and reinforcements of engineering interest.

In this work, we investigate the solidification of Si-rich hypereutectic aluminum–silicon alloy matrix composites, using steady-state directional solidifica-

*Present address: Department of Materials, Swiss Federal Institute of Technology in Lausanne, CH-1015 Lausanne, Switzerland.

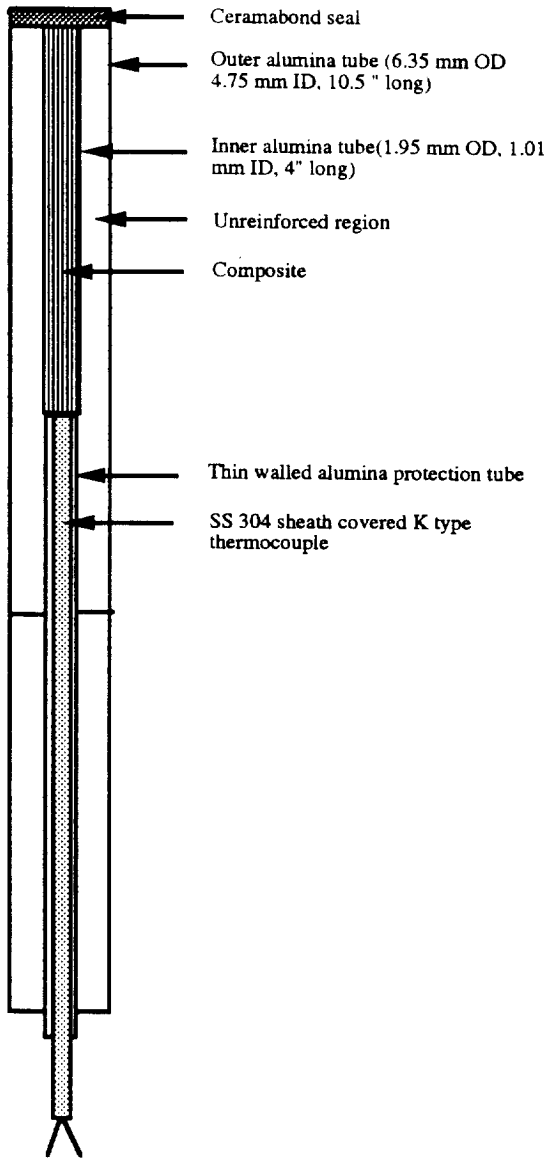

Fig. 1. Cross-section of a container and composite specimen employed in directional solidification experiments.

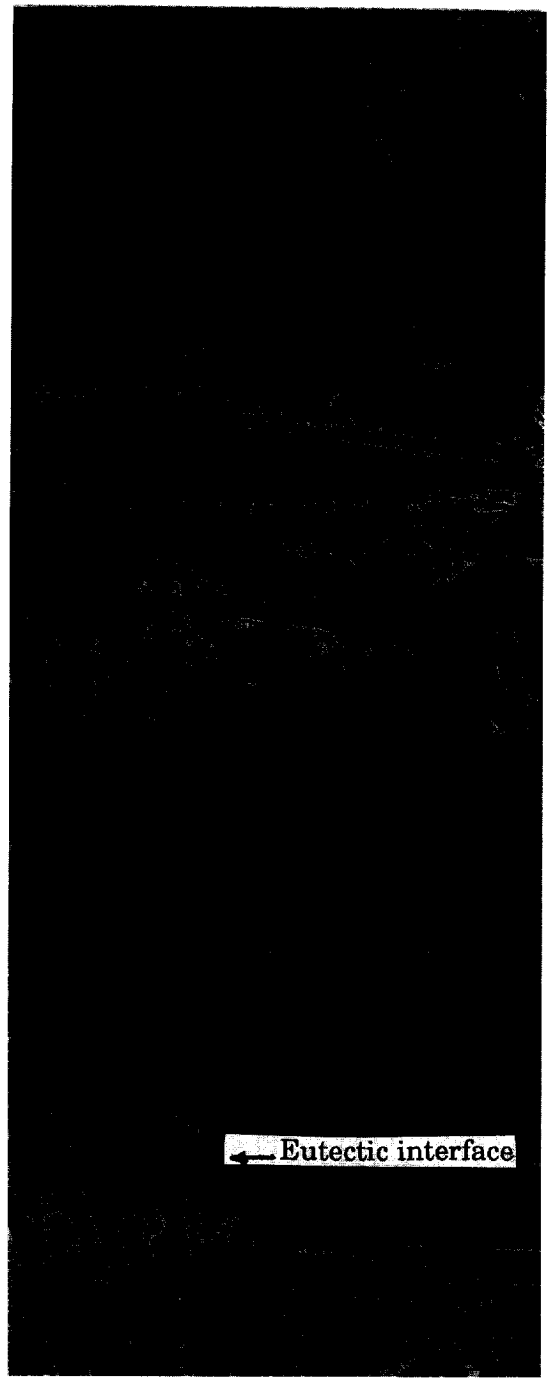

Fig. 2. Photomicrograph of a longitudinal section of a quenched bulk (unreinforced) specimen directionally solidified at 77 μm/s, showing quenched interface.

tion experiments, as we have in the past for Al–Cu alloys. In the unreinforced condition, these alloys are known to grow with various morphologies, which are largely dictated by the tendency of primary Si to exhibit facets along low-energy, atomically smooth, slow-growing (111) planes [8]. Growth along these facets is strongly influenced by the difficulty associated with the formation of new atomic layers. This results in large kinetic undercoolings, and in the occurrence of multiple twins driving the solidification of the primary Si phase, as documented in several studies on the directional solidification of this class of alloys [9–12].

2. EXPERIMENTAL PROCEDURE

Fiber-reinforced composite specimen preparation and casting procedures were similar to those used in an earlier study of alumina fiber-reinforced aluminum–copper alloys [5]. For the production of each sample, about 0.5 g of Fiber FP^{TM} (DuPont de Nemours, Delaware, U.S.A.) α-alumina fibers, 20 μm in diameter, were cut into strands 75 mm

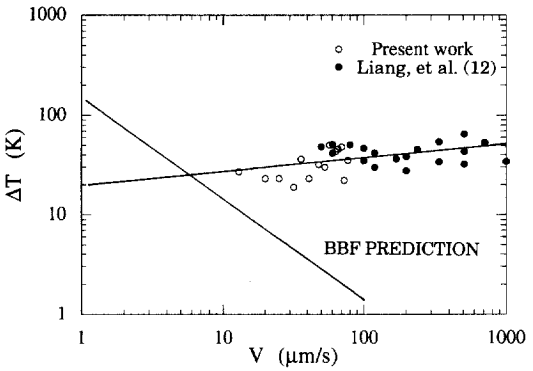

Fig. 3. Primary silicon tip undercooling vs growth velocity for bulk specimens. Data from this study on Al–30 wt% Si, and from Liang *et al.* [12] on Al–18.3 wt% Si, compared with BBF model prediction for Al–30 wt% Si.

long and inserted in the smaller of the two coaxial alumina tubes shown in Fig. 1. The packed fiber preform and thermocouple assembly was then inserted in the larger alumina tube, and the resulting assembly was dried and heated to 1273 K. It was then infiltrated by an Al–30 wt% Si melt prepared from high-purity Al (99.9%) and Si (99.99 + %), using argon pressurized to 3 MPa. After infiltration, the applied gas pressure was maintained during cooling until the temperature of the specimen had dropped below about 833 K, to prevent any dewetting of the fibers.

After fabrication, each infiltrated specimen was directionally solidified in the Bridgman furnace described in Ref. [5]. Samples were solidified over at least 37 mm prior to quenching. At the time of quench approximately 35 mm of infiltrated composite remained liquid in front of the primary silicon tips. Bulk (non-composite) specimens comprised the solidified material in the space between the two alumina tubes (Fig. 1). The growth velocity was varied from 1 to 77 μm/s. The temperature gradient in these experiments was held as constant as possible; measured gradients in individual runs ranged from 15×10^3 to 25×10^3 K/m.

The silicon tip temperature T_t was determined by measuring the distance between the metallographically observed positions of the tip and eutectic isotherms on longitudinal sections, and reporting this distance on the temperature vs distance curves recorded by the thermocouple for each experiment. "Tip temperature" is defined as the isotherm at the leading front of the growing silicon phase. Tip undercooling was then computed as $\Delta T = T_L - T_t$, where T_L is the equilibrium liquidus of the alloy.

3. EXPERIMENTAL RESULTS

Results for the reinforced Al–30% Si alloy are similar to those of Liang *et al.* [12] for Al–18.4 wt% Si. Large, plate-like crystals of primary Si are found, similar to those observed by Liang *et al.* at

Fig. 4. Photomicrograph of a longitudinal section of a quenched composite specimen solidified at 1.2 μm/s, showing eutectic interface.

values of the cooling rate GV less than about 1 K/s (Fig. 2). In the present experiments, cooling rates were in the range of 0.02–1.5 K/s. Also, similar to Liang *et al.*, significant Si macrosegregation was detected in the unreinforced regions of the samples, featuring silicon enrichment near the bottom of the samples. Correspondingly, the liquid near the primary silicon growth front was, especially at lower growth velocities, depleted in Si. Primary Si crystal tip undercoolings reported are based on the actual measured concentration in their vicinity [13], using the same correction method as Liang *et al.* [12]. Results for measured Si crystal tip undercoolings are plotted in Fig. 3. Despite the difference in alloy concentration between the two studies, the measured undercoolings fall on the same curve.

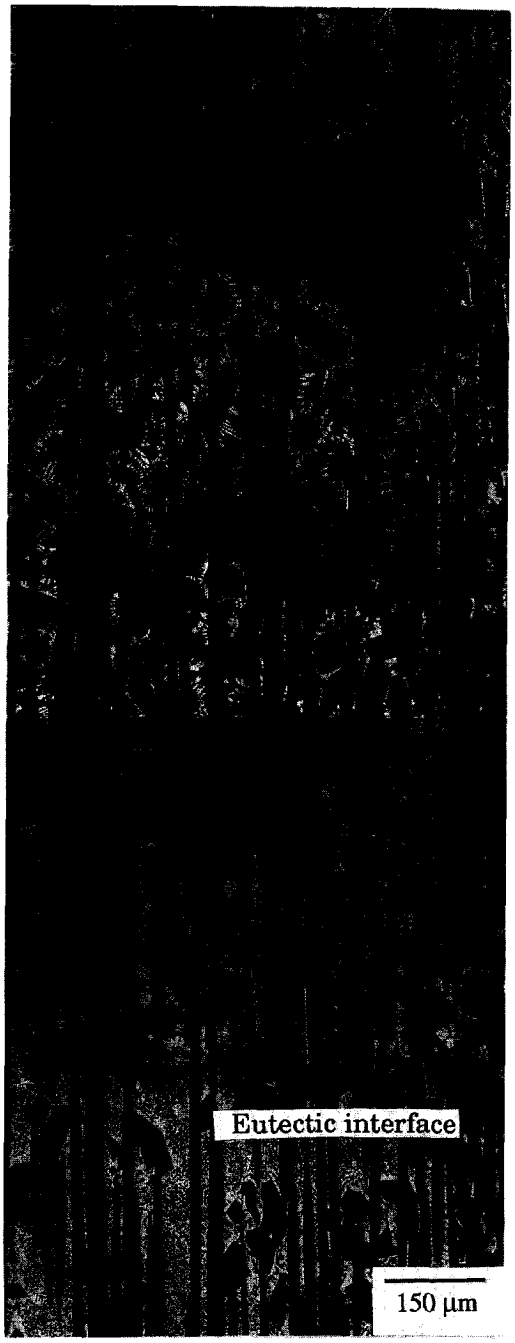

Fig. 5. Photomicrograph of a longitudinal section of a quenched composite specimen solidified at 77 μm/s, showing eutectic interface.

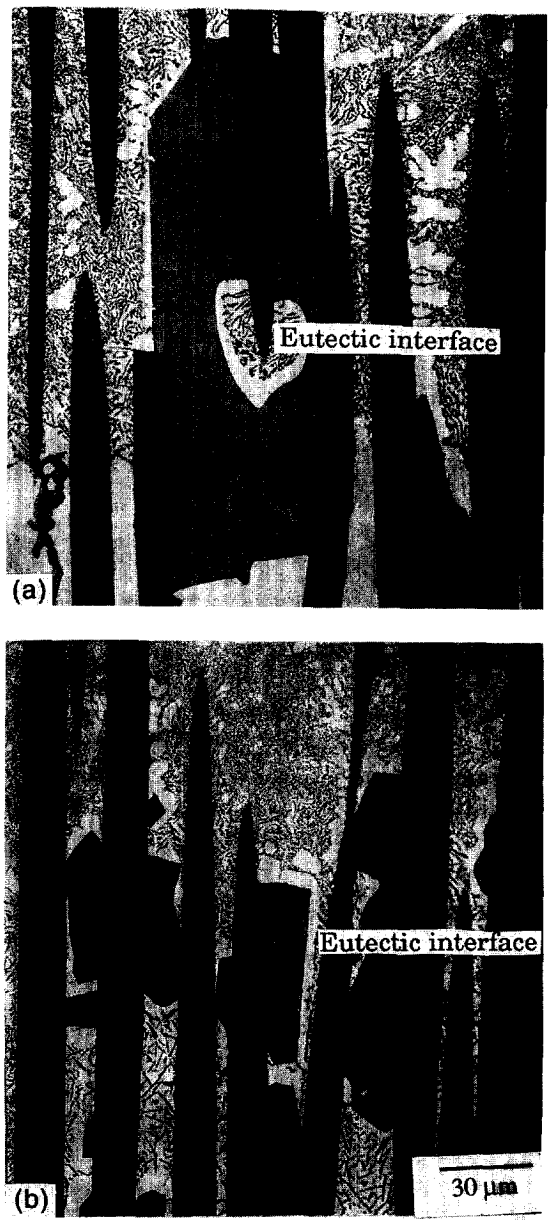

Fig. 6. Magnified view of the eutectic interface in composite specimens solidified at (a) 1.2 μm/s and (b) 77 μm/s; longitudinal sections.

Primary Si crystals in the composite were much smaller than in the unreinforced alloy. Figures 4 and 5 show examples of longitudinal sections from samples solidified at 1.2 μm/s and 77 μm/s, respectively. As velocity increases, the apparent crystal size on the polished surface decreases. Enlarged horizontal and vertical sections are shown in Figs 6 and 7. Facets in many of the apparently isolated Si particles were found to be parallel, indicating that these are in fact connected portions of the same crystal. This observation, quite evident in Fig. 7, was confirmed at a fixed location by successive layer removal by grinding, followed at each step by sample polishing and metallographic examination.

Experimental results on primary Si tip undercooling in the composite specimens are summarized in Fig. 8. No macrosegregation occurred in the liquid in these samples, so this undercooling is simply the equilibrium liquidus temperature for the original alloy, less the observed temperature of the silicon growth front. Note the marked difference in solidification behavior of the alloy, depending on whether

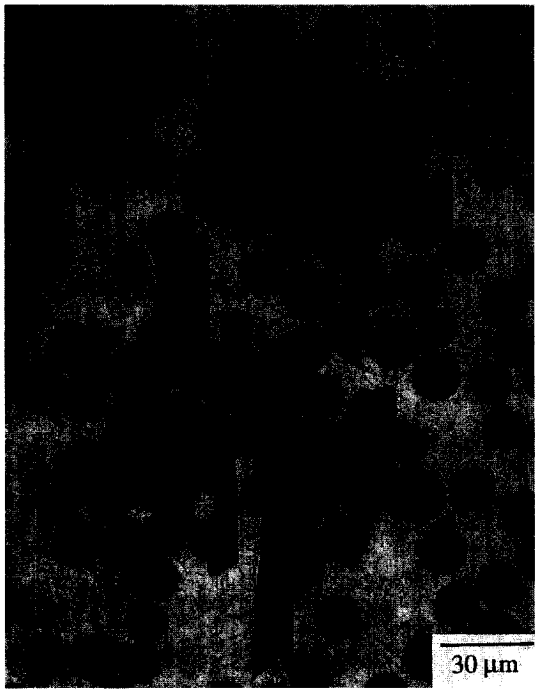

Fig. 7. Photomicrograph of a transverse section of a composite specimen solidified at 12.6 μm/s; sample quenched from within the liquid–solid zone.

it is directionally solidified in bulk (Fig. 3) or in composite form (Fig. 8).

4. DISCUSSION

Cell tip undercoolings in unreinforced non-faceting alloys are known to be well described [14] by the Bower–Brody–Flemings (BBF) equation [15]. This gives the cell tip temperature T_t as equal to:

$$T_t = T_o + \Delta\frac{mC_o(1-k)}{k} \tag{1}$$

where k is the partition ratio, m is the liquidus slope, T_o is the liquidus temperature at the bulk liquid composition C_o, and Δ is the dimensionless cell tip undercooling, equal to

$$\Delta = \Delta_{BBF} \equiv \frac{G}{mG_o} \tag{2}$$

with

$$G_o = \frac{-VC_o(1-k)}{kD} \tag{3}$$

where V is the growth velocity, G the temperature gradient, and D the solute diffusivity in the liquid. In experiments similar to those reported here (on hypoeutectic Al–Cu alloys reinforced with the same alumina fibers), it has been shown that in composites, cell tip undercoolings can significantly exceed the value predicted by the BBF equation [5]. The observed increases in cell tip undercooling were shown to be satisfactorily described by current theories of cell tip solidification, summarized in Ref. [3]. This predicts that, as the parameter N defined by

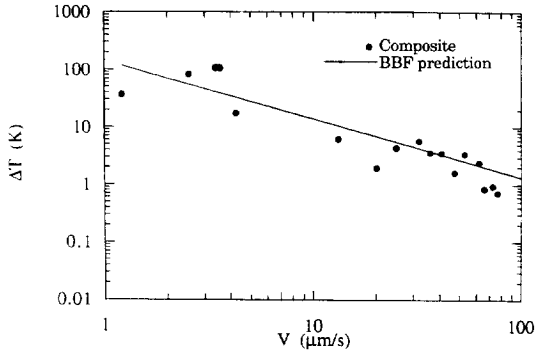

Fig. 8. Primary silicon tip undercoling vs growth velocity for composite specimens. Experimental points compared with BBF model prediction.

$$N = \frac{\Lambda}{2\pi}\sqrt{\frac{mG_o - G}{\Gamma}} \tag{4}$$

falls below about 2, the cell tip undercooling is significantly increased above the value predicted by equation (1). In equation (4), Λ is the average width of the interstice left between fibers and Γ is the Gibbs–Thomson coefficient of the primary phase of the alloy.

With hypereutectic Al–Si alloys, using system parameters given in Appendix I and relevant experimental solidification parameters of $G = 2 \times 10^4$ K/m, 1 μm/s$\geq V \geq$ 77 μm/s, and 10 μm $\geq \Lambda \geq$ 30 μm (corresponding to observed interfiber spacings in the composite microstructure, Fig. 7), calculated values of N fall in the range from 10 to 100.

The high values of N found for the present experiments, despite the narrow interfiber spaces and low values of V, stem from the very low solubility of Al in solid Si, such that k is small and G_o is large [equation (3)]. Provided that predictions from theory developed for non-faceted growth can be extended to the solidification of Si, calculated values of N being far in excess of two, no significant increase in cell tip undercooling above the value predicted by the BBF equation is expected to be caused in the present system by the geometrical contraint imposed on primary Si growth by the fibers. This is substantiated by experiment: comparison between the observed Si crystal tip undercoolings and equation (1) shows good agreement (Fig. 8). Hence, in the presence of fibers, the undercooling at the tip of the polyhedral faceted Si cell is primarily due to solute build-up and diffusion in front of the growing tips.

Agreement with the BBF equation [equation (1)], also implies that in the composite the primary silicon phase grows with no kinetic undercooling. This is in marked contrast with the unreinforced alloy, for which tip undercoolings plotted in Fig. 3 are

compared with predicted values from the BBF equation for Al–30 wt% Si. Here, the observed tip undercooling increases with growth velocity V, and remains far above the value predicted by [equation (1)].

The large Si crystal undercooling observed in the unreinforced alloy is usually interpreted as being a manifestation of significant kinetic undercooling, itself owing to difficulty in forming new stepped layers of solid along the atomically smooth primary Si liquid/solid interface [8, 12, 16]. This interpretation is reinforced by the observation that the high observed Si tip undercoolings in the unreinforced alloy are seemingly independent of Si concentration: comparison with data of Liang *et al.* [12] shows that it is the same at a given velocity regardless of alloy composition.

Metallography indicates that the contact angle θ of the solid Si phase on the fiber in the liquid Al–Si alloy measured through solid Si is finite, and far smaller than that observed in the hypoeutectic Al–Cu system. This is clearly seen at higher magnification in Fig. 7, which shows that in two dimensional cuts through the quenched solidifying microstructure, the contact angle θ assumes a range of values which appear spread roughly equally about $\theta = 90°$ (this was confirmed by examination of fifty contact points in all eight samples). These values of θ are far smaller than those of corresponding angles seen for Al–Cu alloys in Fig. 8 of Ref. [5], which are all very near 180°.

Since it appears unreasonable that the geometrical restriction on growth imposed by the fibers would per se decrease the kinetic undercooling at the tip of the growing Si crystals, the observed elimination of the kinetic undercooling by the fibers must be caused by the comparatively low value of the contact angle θ of the solid Si on the fibers in the liquid. Furthermore, because no drastic reduction in the number of primary Si crystals was observed, and because primary Si crystals were observed to extend over a significant fraction of the sample volume, a mechanism whereby the primary Si crystal undercooling is reduced by repeated nucleation of Si crystals at the fibers is excluded: it is by aiding *growth* of primary Si crystals that the fibers essentially eliminate the primary Si kinetic undercooling. This, in turn, shows that the fibers somehow promote the nucleation of new solid Si atom layers along slow-growing (111) facets, and do so with considerable efficiency.

Primary Si in aluminium is known to grow, at least in many instances, by the twin plane re-entrant angle (TPRE) mechanism [10–12, 17]. In TPRE growth, the nucleation of new layers of solid Si growing along (111) facets is aided at the re-entrant groove defined by contact of two (111) facets and a twin, a second parallel twin being required for self-perpetuation of the mechanism [18–22]. Since primary Si undercoolings measured in the composites

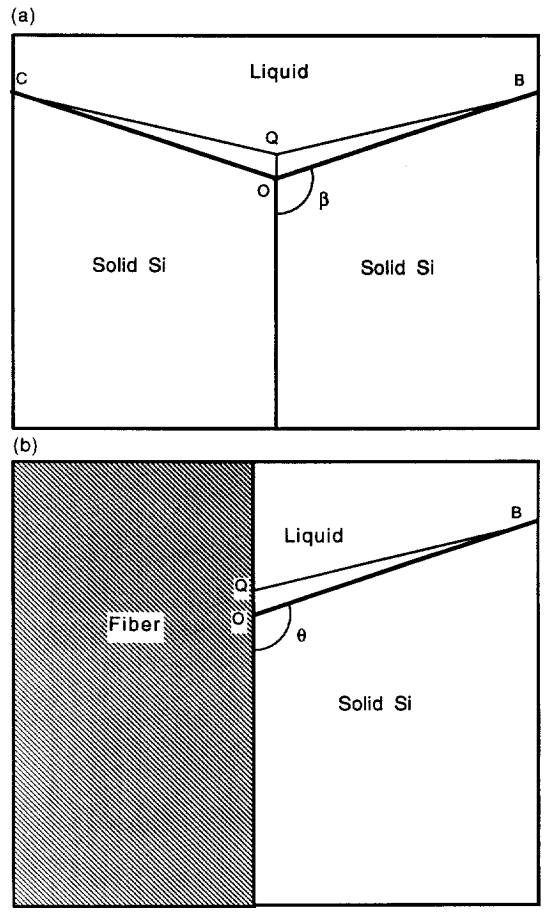

Fig. 9. (a) Sketch of interfaces and incremental triple line motion for derivation of capillaric equilibrium at a re-entrant twin corner; (b) interfaces and incremental triple line motion for derivation of capillary equilibrium at the contact line of the solidification front with a flat foreign surface.

are far lower than for primary silicon in the unreinforced alloy, the heterogeneous (111) facet atom layer nucleation mechanism provided by contact of Si with the fibers is clearly far more efficient than that provided near a re-entrant twin. This result is, at first glance, surprising: indeed, why would contact with a foreign crystalline substance provide a better ledge nucleation site than contact, at a re-entrant groove, with the growing material itself, separated only by a twin which is an interface of very low energy?

We propose that the reason for this difference in ledge formation catalysis between a twin and a foreign surface stems from the fact that capillary forces at a foreign surface can bend the interface between primary Si and the liquid, thus creating a continuous source of pre-existing ledges which can move easily along primary Si facets. Such interface bending is not expected at a twin.

To show this, consider an advancing liquid/solid interface corresponding to an atomically smooth

(111) Si facet, contacting either a twin [Fig. 9 (a)] or a flat fiber surface [Fig. 9 (b)]. Twin boundary energies change in theory infinitely fast with misorientation about the low-energy twin configuration; therefore, the twin surface can be considered rigid in the analysis of capillary equilibrium at the triple line depicted in Fig. 9(a) [23]. Similarly, the fiber surface can be considered rigid, given the chemical inertness and low mobility of fiber atoms at the temperature of the present solidification experiments. Therefore, capillary equilibrium in both configurations is to be analyzed in the plane of the solid/solid interface only. To this end, we use the approach developed by Herring for the analysis of capillary equilibrium at triple lines with anisotropic surface energies [23–25].

Consider first the line of contact between two solid Si crystals separated by a twin, and the liquid [Fig. 9 (a)]. We define as β the angle between the twin and each of the liquid/solid interfaces. The change in free energy accompanying displacement of the liquid/solid interface by an infinitesimal distance OQ about two points B and C equidistant from O and located along the liquid/solid interface far from O is

$$\frac{\delta A}{\mathrm{OQ}} = \sigma_{\mathrm{twin}} + 2\cos(\beta)\sigma_{\mathrm{sl}} - 2\sin(\beta)\frac{\partial \sigma_{\mathrm{sl}}}{\partial \beta} \qquad (5)$$

where σ denotes interfacial energy, and subscripts "twin" and "sl" denote twin and solid/liquid interfaces, respectively (the notation used in Fig. 9 is chosen so that this result can be obtained directly from the exposition of Herring's derivation by Lupis in Ref. [25], p. 378).

Similarly, the corresponding change in free energy for a similar motion of the triple line of contact between solid Si, the liquid, and the fiber surface [Fig. 9(b)] from O to Q by rotation of the liquid/solid interface about point B far from O is

$$\frac{\delta A}{\mathrm{OQ}} = \sigma_{\mathrm{sf}} - \sigma_{\mathrm{lf}} + \cos(\theta)\sigma_{\mathrm{sl}} - \sin(\theta)\frac{\partial \sigma_{\mathrm{sl}}}{\partial \theta} \qquad (6)$$

if θ is the angle of contact of Si on the fiber in the presence of the liquid, measured through the solid, and σ_{sf} and σ_{lf} denote interfacial energies between the fiber and solid Si, and the fiber and liquid, respectively.

At equilibrium, in each of the two situations, we therefore have:

$$\frac{\sigma_{\mathrm{twin}}}{2} = -\cos(\beta)\sigma_{\mathrm{sl}} + \sin(\beta)\frac{\partial \sigma_{\mathrm{sl}}}{\partial \beta} \qquad (7)$$

and

$$\sigma_{\mathrm{lf}} - \sigma_{\mathrm{sf}} = \cos(\theta)\sigma_{\mathrm{sl}} - \sin(\theta)\frac{\partial \sigma_{\mathrm{sl}}}{\partial \theta} \qquad (8)$$

respectively. Equation (8) is in fact the generalization to the case of anisotropic interfacial energies of the classical Young–Dupré equation. The last term on the right-hand side of both equations represents the equivalent of a torque acting on the liquid/solid interface, tending to rotate the interface towards directions of low interfacial energy.

The value of the rate of change of the solid Si/liquid interfacial energy with orientation, $(\partial\sigma_{\mathrm{sl}}/\partial\alpha)_{\alpha=0}$ with α denoting the misorientation angle from (111), can be obtained by assimilating orientations slightly different from (111) to a smooth (111) plane containing a few parallel ledges of height h and appropriate spacing d [24]. The energy of such a plane is

$$\sigma_{\mathrm{sf}} = \sigma_{(111)} + \alpha\sigma_{\mathrm{ledge}} \qquad (9)$$

with $\alpha = h/d$; σ_{ledge} is the interfacial energy along the ledge surface. Since we expect σ_{ledge} to be at least of the same order of magnitude as $\sigma_{(111)}$, this simple model leads to the conclusion that at orientations differing slightly from (111), $(\partial\sigma_{\mathrm{sl}}/\partial\alpha)$ is about as large as $\sigma_{(111)}$.

Where the curve plotting σ_{sl} as a function of orientation α displays a cusp, as is the case when the solid/liquid interface has precisely the (111) orientation, $(\partial\sigma_{\mathrm{sl}}/\partial\alpha)$ is indeterminate, being situated somewhere between its maximal absolute value in each orientation. The liquid/solid interface oriented along a (111) plane will therefore remain stable at O in the two configurations of Fig. 9(a) and (b) as long as this maximal absolute value of the energy increase owing to rotation of the liquid/solid interface exceeds any lowering in interfacial energy that may result from interface creation and annihilation accompanying marginal changes in β or θ [equations (5) and (6)].

Consider first the situation, typically depicted when the TPRE mechanism is described in the literature [e.g. 18], where two (111) facets meet at a twin. The angle of contact is then given by crystallography, and is such that, in the diamond structure of Si, $\beta = 109.5°$ [18]. $\mathrm{Cos}(\beta)$ and $\sin(\beta)$ then equal (−0.033) and 0.943, respectively. The twin boundary energy, σ_{twin}, is expected to be far lower than σ_{sl}, and since σ_{111} is of the same order of magnitude as the maximum value of $(\partial\sigma_{\mathrm{sl}}/\partial\beta)$, equation (7) shows that the configuration of two atomically smooth (111) planes meeting at a twin, generally postulated in analysis of the TPRE growth mechanism [e.g. 18] is thermodynamically stable because of the anisotropy of σ_{sl} (this is contrary to the situation where a twin meets a free surface of isotropic energy, in which case capillary forces create a rounded transition between the macroscopic free surface orientation, and the orientation dictated by capillary equilibrium of isotropic free energies according to the classical dihedral angle equation [26]).

Consider now the case of an atomically smooth (111) liquid/solid interface plane meeting a foreign surface [Fig. 9 (b)]. Depending on the value of the angle of contact θ of the solid Si phase with the

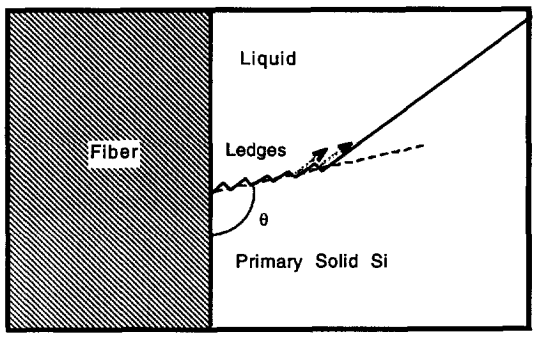

Fig. 10. Ledge formation caused by liquid–solid interface bending under the action of capillary forces near the line of contact of a growing facetted solid with a solid substrate.

foreign surface along the (111) plane in question, $\cos(\theta)$ may be smaller or larger than $\sin(\theta)$. Furthermore, $\sigma_{lf}-\sigma_{sf}$ is expected, contrary to σ_{twin}, to assume a significant value, on a par with that of σ_{sl}: there is a significant difference in chemical nature between the fiber/liquid and the fiber/solid interfaces, and alumina is known to catalyze nucleation of primary Si with some efficiency [2]. It is therefore expected, at least for certain values of σ, that the capillary equilibrium equation, equation (8), will be violated for liquid/solid interfaces which remain oriented along (111) at the line of contact with a foreign surface. When this is the case, near the foreign surface, capillary forces exceed the resistance to interface orientation away from (111), and cause bending of the liquid/solid interface away from the (111) orientation, towards a different orientation which satisfies equation (8) at the triple line. Since, along the line of intersection of a (111) plane and a fiber, θ assumes a range of values, which is further increased by the roughness present along the surface of Fiber FP™ fibers, primary Si/liquid interfaces bent in both directions away from (111) should be formed near the fibers.

Such bent interfaces in the vicinity of fiber/primary Si/liquid triple lines are in fact evident in micrographs taken along the quenched region ahead of the eutectic front (Figs 6 and 7). Their existence, which is thus explained by capillarity, implies that fiber surfaces can create concave regions of liquid/solid interface oriented away from the (111) orientation. Such concave liquid/solid interface regions provide a location at which new ledges are continuously present, and from which new layers can propagate across the liquid/solid interface, as depicted schematically in Fig. 10. The presence of fibers should thus eliminate the need for nucleation of new layers along (111) facets of growing primary Si crystals, in turn reducing the otherwise significant interfacial kinetic undercooling of growing primary Si to negligible values.

Comparatively, experimental data suggest that re-entrant twin planes provide a far less efficient source of new Si layers along (111) planes. Indeed, although twins provide a line of atomic positions where atoms can attach with greater ease to the growing crystal than along a flat facet [20–22], the twin provides only a means for lowering somewhat the formation energy of a nucleus of critical size, which in this mechanism must still form for each new crystal layer to grow. More work is clearly required to understand quantitatively the kinetics of growth by the TPRE mechanism; however, we note that the tentative conclusion reached here may explain why it was found in Refs [10, 11] that twinned and untwinned primary Si crystals coexist in directionally hypereutectic Al–Si alloys. Indeed, this observation indicates that the presence of twins, although offering an elegant rationalization of the shape of crystals formed in several systems [18, 19, 22, 27–29], and shown to increase the rate of crystal growth in one system (submicron platinum crystals coarsening in an oxidative vapour phase) [30], does not dramatically decrease the kinetic undercooling of primary Si crystals growing in Al–Si alloys.

5. CONCLUSIONS

A large velocity-dependent undercooling is measured in the directional solidification of primary Si growing from Al–30 wt% Si at velocities between 1 and 77 μm/s. This undercooling is found to display the same functional relationship to velocity as was measured by Liang *et al.* in directionally solidified Al–18.7 wt% Si, indicating that it is kinetic in nature. In all likelihood, this undercooling results from difficulty in nucleation of new atomic planes along slow-growing (111) facets.

Continuous aluminum oxide fibers essentially eliminate this kinetic undercooling during directional solificication: in the same velocity range, the undercooling at the tip of primary Si crystals is entirely accounted for by the Bower–Brody–Flemings equation. In the composite, the undercooling is therefore solutal in nature.

The elimination of all kinetic undercooling by the fibers is explained as being a result of capillary forces bending the liquid/solid interface near the contact line of (111) facets with the fibers. This bending causes the formation of a permanent source of ledges along slow-growing (111) facets, thus eliminating the need to nucleate new atomic plane layers. This feature is shown to be absent at twin plane re-entrant angles, indicating that twin plane pairs provide a far less efficient ledge formation site than a foreign surface along slow-growing (111) facets in hypereutectic Al–Si alloys.

Acknowledgements—This work was supported by the National Science Foundation, Grant #DMR-9113679

REFERENCES

1. Trivedi, R., Han, S. H. and Sekhar, J. A., in *Proc. Conf. on Solidification of Metal-Matrix Composites*, ed. P. K. Rohatgi. TMS-AIME, Warrendale, PA 1989, pp. 23–37.
2. Mortensen, A. and Jin, I., *Int. Mater. Rev.*, 1992, **37**, 101.
3. Mortensen, A., *Mater. Sci. Engng*, 1993, **A173**, 205.
4. Mortensen, A. and Flemings, M. C., *Metall. Trans.*, 1995, **27A**, 595.
5. Dean, N. F., Mortensen, A. and Flemings, M. C., *Metall. Trans.*, 1995, **26A**, 2141.
6. Mortensen, A., Cornie, J. A. and Flemings, M. C., *Metall. Trans.*, 1988, **19A**, 709.
7. Wang, W., Ajersch, F. and Löfvander, J. P. A., *Mater. Sci. Engng*, 1994, **A187**, 65.
8. Flemings, M. C., *Solidification Processing*. McGraw-Hill, New York, 1974, 319–324.
9. Steen, H. A. H. and Hellawell, A., *Acta metall.*, 1972, **20**, 363.
10. Atasoy, O. A., Yilmaz, F. and Elliot, R., *J. Cryst. Growth*, 1984, **66**, 137.
11. Yilmaz, F., Atasoy, O. A. and Elliott, R., *J. Cryst. Growth*, 1992, **118**, 377.
12. Liang, D., Bayraktar, Y. and Jones, H., *Acta metall. mater.*, 1995, **43**, 579.
13. Sundarrajan A. *Solidification behavior of Al–30 wt% Si in the presence of continuous alumina fibers*. Ph.D. thesis. Department of Materials Science and Engineering, Massachusetts Institute of Technology, 1996.
14. Billia, B. and Trivedi, R., in *Handbook of Crystal Growth—Part 1b—Fundamentals—Transport and Stability*, ed. D. T. J. Hurle. North-Holland. Amsterdam 1993, pp. 899–1073.
15. Bower, T. F., Brody, H. D. and Flemings, M. C., *Trans. Metall. Soc. AIME*, 1966, **236**, 624.
16. Tiller, W. A., *The Science of Crystallization—Microscopic Interfacial Phenomena*. Cambridge University Press, Cambridge, 1991, pp. 37–92.
17. Granger, D. A. and Elliott, R., in *Metals Handbook Ninth Edition—Vol. 15, Casting*, ed. D. M. Stefanescu. ASM International, Metals Park, OH, 1988, pp. 159–168.
18. Hamilton, D. R. and Seidensticker, R. G., *J. Appl. Phys.*, 1960, **31**, 1165.
19. Wagner, R. S., *Acta metall.*, 1960, **8**, 57.
20. Ming, N. B. and Sunagawa, I., *J. Cryst. Growth*, 1988, **87**, 13.
21. Li, H., Peng, X. D. and Ming, N. B., *J. Crystal. Growth*, 1994, **139**, 129.
22. van de Waal, B. W., *J. Cryst. Growth*, 1996, **158**, 153.
23. Herring, C., in *Structure and Properties of Solid Surfaces*, ed. R. Gomer and C. S. Smith. The University of Chicago Press, Chicago, IL, 1952, pp. 5–81.
24. Mullins, W. W., in *Metal Surfaces: Structure, Energetics and Kinetics*. American Society for Metals, Metals Park, OH, 1963, pp. 17–66.
25. Lupis, C. H. P., *Chemical Thermodynamics of Materials*. North-Holland, Elsevier, New York, Amsterdam, 1983, p. 378.
26. Shewmon, P. G. and Robertson, W. M., in *Metal Surfaces: Structure, Energetics and Kinetics*, American Society for Metals, Metals Park, OH, 1963, pp. 67–98.
27. Morris, R. H., Bottoms, W. R. and Peacock, R. G., *J. Appl. Phys.*, 1968, **39**, 3016.
28. Kitamura, M., Hosoya, S. and Sunagawa, I., *J. Cryst. Growth*, 1979, **47**, 93.
29. Li, D., Eckler, K. and Herlach, D. M., *J. Cryst. Growth*, 1996, **160**, 59.
30. Harris, P. J. F., *J. Catalysis*, 1986, **97**, 527.
31. Kurz, W. and Fisher, D. J., *Fundamentals of Solidification* 3rd edn. Trans Tech Publications, Aedermannsdorf, Switzerland, 1989, p. 294.

APPENDIX

Thermophysical Properties for Hypereutectic Al–Si Alloys

k partition ratio $= 2 \times 10^{-4}$ [31].

m liquidus slope $= -13.39$ K/wt%, from a straight-line approximation of the Si/Al–Si liquidus between 810°C and 577°C.

Γ Gibbs–Thomson coefficient $= 1.7 \times 10^{-7}$ K m [31, p. 294].

D Si diffusion coefficient in liquid Al $= 2.08 \times 10^{-7} \exp(25740/8.32\,T)$ m^2/s where T is temperature in K [12]. Near 700°C, $D = 0.9 \times 10^{-8}$ m^2/s.